PASJ: Publ. Astron. Soc. Japan **52**, 847–865 (2000)

Stellar Contents of the Galactic Giant H II Region NGC 3603

Anil K. PANDEY
Uttar Pradesh State Observatory, Manora Peak, Naini Tal 263 129, India
E-mail (akp): pandey@upso.ernet.in

Katsuo OGURA
Kokugakuin University, Higashi, Shibuya-ku, Tokyo 150-8440
and
Kaz SEKIGUCHI
Subaru Telescope, National Astronomical Observatory of Japan, 650 North A'ohoku Place, Hilo, Hawaii 96720, U.S.A.

(Received 1999 July 22; accepted 2000 July 8)

Abstract

We present CCD $UBVRI$ and Hα photometry for the starburst cluster associated with the galactic giant H II region NGC 3603. The mean reddening of the cluster members comes out to be $\langle E(B-V)\rangle = 1.48\pm0.21$ (s.d.). The surface distribution of the reddening shows a radial variation with a minimum near to the cluster center and two local maxima at radii $\sim 30''$ and $\sim 70''$. Our photometric data indicate an anomalous reddening law for the dust inside the cluster region, and the ratio of the total to the selective extinction, R, is found to be ~ 4.3. A comparison of the observational and intrinsic colour-magnitude digrams (CMDs) yields a mean distance modulus of $(m-M)_0 = 14.0$, which corresponds to a distance of 6.3 ± 0.6 kpc. This distance is smaller than those obtained in earlier works (e.g., 7.2 kpc, Melnick et al. 1989, AAA 49.132.013) but is in good agreement with the kinematic distance (6.1 ± 0.6 kpc) recently reported by De Pree et al. (1999, AAA 71.132.041). The cluster shows a large age spread, containing stars as old as up to several Myr. However, the mean age of the cluster is found to be ≤ 1 Myr. We estimate a minimum star formation efficiency of $\sim 25\%$ and a gas removal time of $\tau \sim 4.6$ Myr.

Key words: open clusters: individual (NGC 3603) — reddenning law — stars: mass function

1. Introduction

Very young star clusters (age < 10 Myr) which are still associated with dense gas and dust clouds provide an opportunity to study the star-formation process in star clusters, because they represent the first stage in the evolution of young stellar complexes. The galactic giant H II region NGC 3603 (G296.1 − 0.5) contains such an object, where star formation is probably an on-going process (Persi et al. 1985; Melnick et al. 1989; Clayton 1990). It is a unique object; it is often described as the most massive, optically visible giant H II region in the Galaxy (Goss, Radhakrishnan 1969). It harbours and is ionized by a starburst cluster which contains a large number of massive stars, including the very compact trapezium-type system HD 97950; recent HST observations by Drissen et al. (1995) have identified three WR stars, six O3 stars, and a dozen early O stars within 0.3 pc. In many aspects NGC 3603 resembles the 30 Dor Nebula in the LMC, which is also associated with the rich cluster NGC 2070, having again the compact, superluminous stellar system R 136a. Compared to the 30 Dor system, NGC 3603 is of slightly smaller scale in both stellar mass and H II gas content, but is more compact (Moffat et al. 1985; Hofmann et al. 1995). Because no other giant H II regions can be studied in detail, even with HST, on account of large distances, NGC 3603 and 30 Dor are extremely important for understanding extragalactic giant H II regions, and even starburst galaxies.

Photometry for NGC 3603 has been reported by Sher (1965), van den Bergh (1978), Melnick and Grosbøl (1982), and Melnick et al. (1989). The core object, HD 97950, has been (partially) resolved with speckle masking observations by Hofmann et al. (1995) and with HST (before refurbishing) by Moffat et al. (1994), both of which provided photometric information on the components of HD 97950. Among these studies, the CCD UBV photometry of Melnick et al. (1989) presented detailed photometric properties of the cluster, such as a large range of the amount of interstellar reddening of 1.3 to 2.0 in $E(B-V)$ and an age of 2 to 3 Myr with an age spread of up to ±2 Myr. Recently, Eisenhauer et al. (1998) presented their results based on near-infrared adaptive optics imaging of the cluster. They found evi-

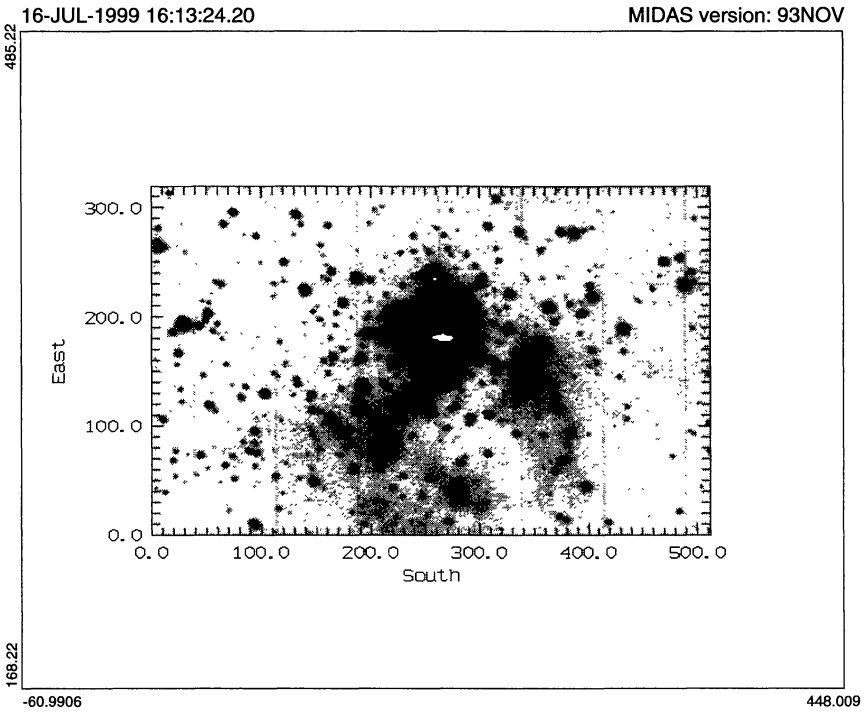

Fig. 1. I band image of the cluster NGC 3603 cluster in a logarithmic stretch.

dence for the presence of stars down to 1 $M_{\odot}$. They also found that the age of the cluster lies between 0.3 and 1 Myr.

In spite of its importance, the distance of NGC 3603 has not been firmly established and has been a subject of controversy, starting with the photometric distance of 3.5 kpc obtained by Sher (1965) and the kinematic determination of 8.4 kpc by Goss and Radhakrishnan (1969). In many recent studies on NGC 3603, a distance of 7 kpc has been adopted, which was derived by Moffat (1983, 7.0 ± 0.5 kpc) and Melnick et al. (1989, 7.2 kpc). However, none of the distance determinations made so far based on photometric data discussed the ratio of the total-to-selective extinction $R = A_V/E(B-V)$ in this region, which is an important quantity that must be accurately known to determine distances photometrically; all of them simply assumed the standard value of $R = 3.1$ or 3.2.

Neckel and Chini (1981) and Chini and Krügel (1983) found evidence for an abnormal interstellar extinction law in several H II regions. The normal extinction law is characterized by $R = 3.1$, whereas $JHKL$ photometry of heavily reddened early type stars in M 16, M 17, and NGC 6334/6357 indicates higher-than-normal colour-excess ratios resulting in abnormal extinction laws with R values of 4.8, 4.9, and 3.7 respectively (Chini, Krügel 1983).

Although the results from HST and adaptive optics observations are now available, they cover only the central region of the cluster ($\sim 30''$ and $\sim 25''$ from the cluster center, respectively). Actually, Eisenhauer et al. (1998) found that the star density did not converge towards larger radii in their field, and that many of the stars near to the edges are still cluster members. In the present work we report our observations in a relatively larger area having a radius of $\sim 90''$. The primary aim of the present paper is to examine the value of R in this region and to thus determine a more reliable distance of NGC 3603 based on our own CCD $UBVRI$ and Hα photometry of the associated cluster. Figure 1 shows our I band image of the NGC 3603 cluster.

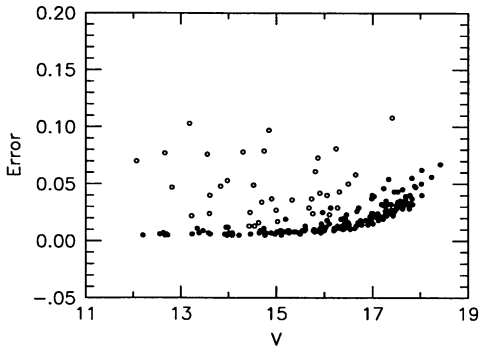

Fig. 2. Errors in the V band as a function of the magnitude for the whole sample. The data points shown by open circles were not included in the analysis.

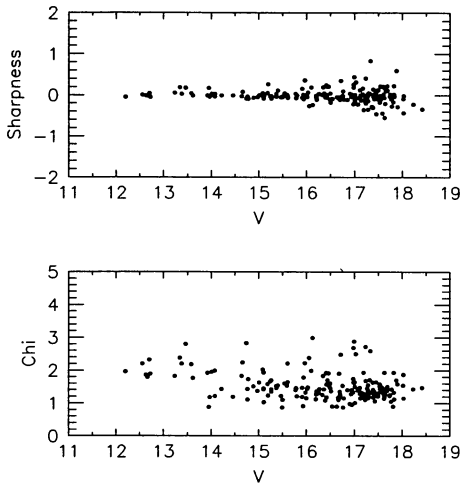

Fig. 3. χ and *Sharpness* parameters for the measurements used in the analysis.

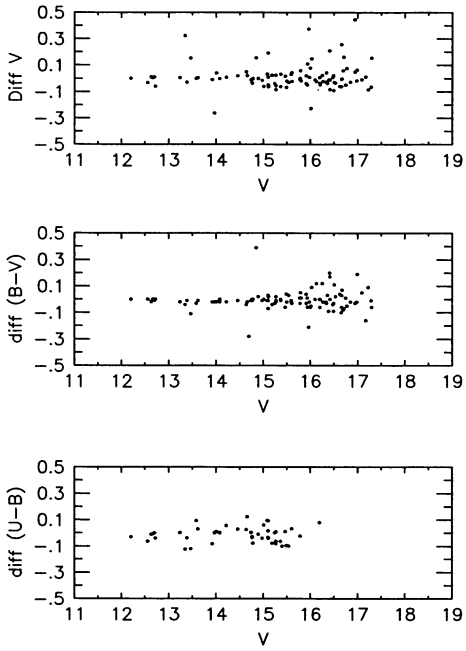

Fig. 4. Comparison between the present CCD photometry and that given by Melnick et al. (1989).

2. Observations and Data Reduction

CCD imaging observations of the NGC 3603 cluster were carried out behind U, B, V, R_c, and I_c band filters and narrow band filters on and just off Hα with the 1.0 m telescope of the South African Astronomical Observatory on 1994 April 3. The camera used a RCA CCD chip having 320 × 512 pixels, each pixel corresponding to 0.″39 at the $f/16$ Cassegrain focus of the telescope. The exposure times were 900, 600, 450, 300, and 300 s in the U, B, V, R_c, and I_c bands, respectively, and 300 s each for both narrow-band filters. The seeing size was 1.″25, judged from the FWHM of the star images of ~ 3.2 pixels. The photometric measurements of the stars were performed using the DAOPHOT II profile fitting software at UPSO. The correction for the nebular contribution was performed by subtracting the nearby background. Transformations to the standard UBV system were obtained by using the UBV magnitudes given by Melnick et al. (1989). The resultant photometric data as well as the positions of the stars measured in NGC 3603 are given in tables 1a and b. These tables are available from the authors in electronic form. The colours, $(v-i)$ and $(v-r)$, are given in the instrumental system. These colours are used to investigate whether the extinction law in the NGC 3603 region is normal or anomalous (see section 5).

Profile-fitting photometry gives the error in the magnitude determination, the goodness of the fit parameter, χ, which is a measure of the average rms deviation to the PSF fit normalized to the expected errors. It also gives a shape parameter, *Sharpness*, which measures how well the PSF fits the object. Figure 2 shows the errors in the V band as a function of the magnitude for the whole sample. Figure 2 shows that a few bright stars have large errors. We find that most of such stars are in the central region of the cluster. Since NGC 3603 is a crowded cluster, and is embedded in a clumpy nebulous region, it is somewhat difficult to obtain reliable photometry in the central region (cf. Selman et al. 1999). Therefore, we constrained our measurements according to DAOPHOT errors. The data points shown by open circles in figure 2 were not included in further analysis. The corresponding parameters, χ and *Sharpness*, for the measurements are shown in figure 3.

Figure 4 shows a comparison between the present CCD

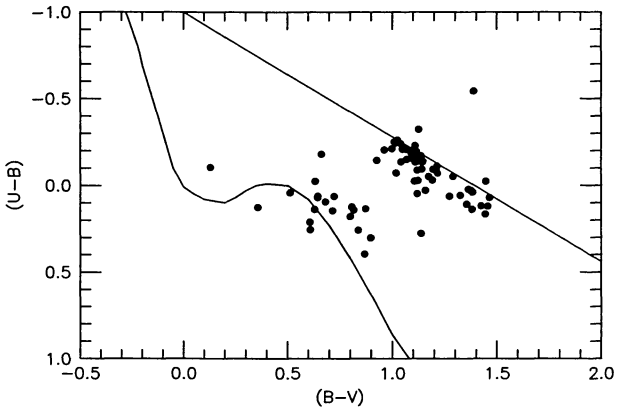

Fig. 5. The $(U-B, B-V)$ diagram for the stars in the cluster region. The curve and the straight line represent the main sequence and the slope of the reddening of 0.71, respectively.

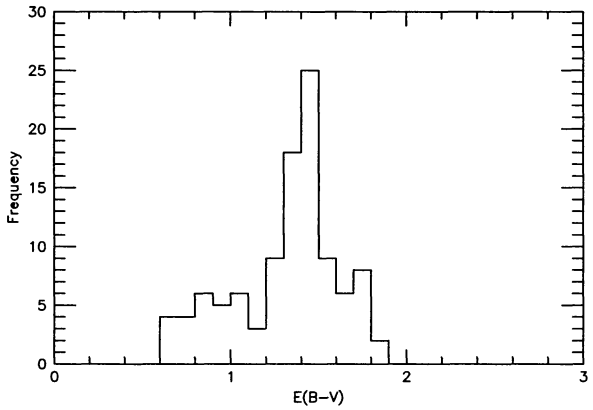

Fig. 6. Frequency distribution of the $E(B-V)$ values for all stars.

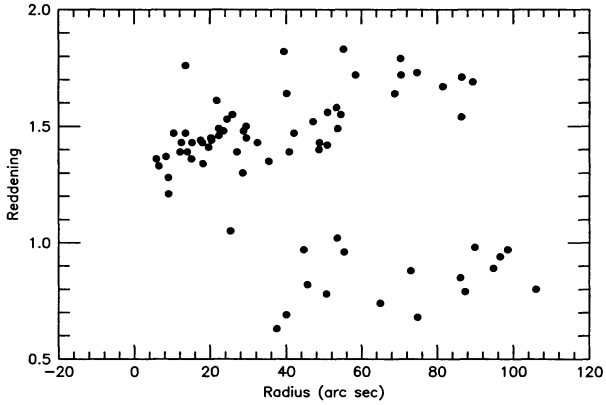

Fig. 7. Radial variation of the reddening $E(B-V)$ in the cluster field.

photometry and the CCD photometry given by Melnick et al. (1989). The plot reveals an overall good agreement between the two photometric measurements, although the scatter increases for stars with $V > 15.0$.

3. Extinction

The amount of interstellar extinction of the stars in the cluster region can be estimated from the $(U-B, B-V)$ diagram displayed in figure 5. The diagram shows that field stars are well separated from the cluster stars, which are distributed nearly along the reddening line. The ZAMS has been taken from Mermilliod (1981). Moffat (1983) obtained the MK spectral classification for nine stars in the cluster. Using the intrinsic colours given by Schmidt-Kaler (1982) and our photometry, we obtained the ratio of the colour excesses, $X = \langle E(U-B)/E(B-V)\rangle = 0.71 \pm 0.01$ (s.d.), for the probable cluster members, which is almost identical with the normal value of 0.72. This slope is shown in figure 5. The interstellar extinction for individual stars was derived using the Q-method (Johnson, Morgan 1953). The $E(B-V)$ values derived for eight stars using the Q-method agree fairly well with those obtained from spectral classification. A comparison (spectroscopic–present) shows that $\Delta E(B-V) = -0.03 \pm 0.04$ (s.d.). The frequency distribution of the $E(B-V)$ values is shown in figure 6. The mean colour excess of the probable cluster members within the radius of 50″ is estimated to be $\langle E(B-V)\rangle = 1.41 \pm 0.13$ (s.d.). For all probable member stars in the whole area of the CCD frame, $\langle E(B-V)\rangle = 1.48 \pm 0.21$ (s.d.) is derived. These values are in good agreement with those estimated by Melnick et al. (1989).

The radial variation of the amount of reddening in the cluster field is shown in figure 7; the cluster center is assumed to be HD 97950. A remarkable feature of the diagram is the variation with two local maxima at radii of $\sim 30''$ and $\sim 70''$. This was not observed in a similar diagram made by Melnick et al. (1989), and appears to imply that the central part of NGC 3603 is surrounded by two dust shells of radii $\sim 30''$ and $\sim 70''$. In the radius range of 10″ to 40″, three stars are noticeable with their high reddening values compared to the other stars in the same radius range. Possible explanations for this may be the following. One star (no. 98) shows Hα emission, as judged from its excess in Hα– continuum magnitude, and may have a circumstellar shell around it. The remaining two (nos. 172, 191) might be background stars.

The projected radial counts of stars for different magnitude ranges have been made in different annuli at increasing distances from the cluster center. The projected radial stellar density is obtained by dividing the number of stars in each annuli by its area, and is shown in figure 8 (in arbitrary units). The noticeable feature of figure 8 is

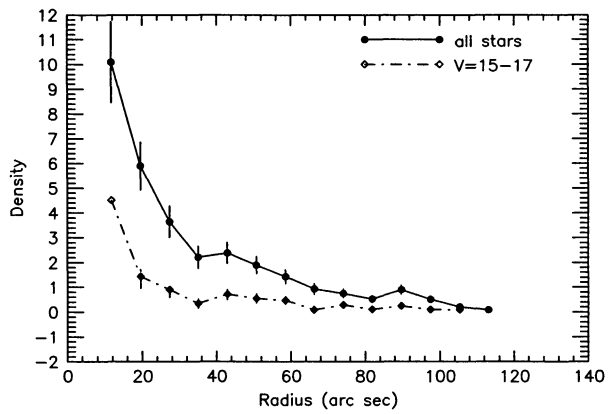

Fig. 8. Radial variation of the projected stellar density for all stars (solid line) and for those with $15 \leq V \leq 17$ (dashed line).

the local maxima at radii $\sim 40''$ and $\sim 90''$, which coincide with the minima of figure 7. The complimentary nature (although rather weak) of figures 7 and 8 supports the validity of the curves of either one.

4. Cluster Membership

As discussed earlier, cluster stars are clearly separated from field stars in the $(U-B,\ B-V)$ diagram. The most reliable method for membership determination is a proper-motion survey, for which we do not have data. There are several photometric methods of estimating cluster membership, and we apply each of them to our data. These methods are:

1) The expected range of colour excess within the cluster. The foreground reddening can be estimated from figures 5 and 7 as well as from figures 10a and 10b (see section 5). Figure 5 shows that the least reddened cluster stars have $(B-V) \sim 0.8$ and that their intrinsic $(B-V)$ values are around -0.30. This indicates a foreground $E(B-V)$ of ~ 1.1. Figure 7 also suggests a foreground $E(B-V)$ of ~ 1.1. The membership of the stars is decided on the basis of their reddening as well as distance from the cluster center. Stars following the 'extinction–radius trend' (as shown in figure 7) and lying within a radius of $60''$, are presumed to be probable cluster members. Those stars having $E(B-V) \sim 1.1$, but not following the trend, may be cluster members lying on the edge of the cloud. The stars having $E(B-V) < 1.1$ are most probably foreground objects.

2) Ogura and Ishida's method (cf. Ogura, Ishida 1981), or P–Q diagrams, where the extinction free magnitude $P = V - R(B-V)$ is plotted against a reddening-free colour $Q = (U-B) - X(B-V)$. This method was successfully applied to the Rosette Nebula cluster (NGC 2244) to avoid any confusion due to differential extinction. We drew several P–Q diagrams with $R = 3.1$ to 6.0. The value of X is taken to be 0.71. The probable cluster sequence stars were selected for each P–Q diagram and it was found that the result was almost the same in each case.

3) Two-colour diagrams (TCDs) of the form $(V-Y)$ vs $(B-V)$, where Y denotes one of the broad band magnitudes from 0.7 to 3.7 μm, i.e., R, I, J, H, K, and L. This method and the results are described in the following section.

The membership of cluster stars is estimated using these methods; the results are given in the last column of table 1a.

5. The Extinction Law

5.1. *Two Colour Diagrams*

The extinction law is indispensable in obtaining the extinction corrected magnitude. Melnick et al. (1989) assumed $R = A_V/E(B-V) = 3.2$ and justified the use of this value by the fact that there was no reported evidence for an abnormal value of R in the region of NGC 3603. Numerous investigations have shown that the normal reddening law with $R = 3.1$ is valid in many parts of our Galaxy. However, H II regions associated with a large amount of gas and dust often show larger values of R (Chini, Krügel 1983 and references therein; Chini, Wargau 1990). It has been shown by Chini and Wargau (1990) that two-colour diagram (TCD) of the form $(V-Y)$ vs $(B-V)$ provides an effective method for separating the influence of the normal extinction produced by the general interstellar medium from that of abnormal extinction arising within regions having peculiar distributions of dust sizes. In other words, these TCDs can distinguish between foreground stars (reddened by normal dust) and the stars embedded in such regions (affected in addition by a special reddening law). On these diagrams the unreddened main sequence and the path of the normal reddening make practically identical lines. This makes these diagrams useless for determining the amount of reddening, but, instead, very useful for detecting anomalies in the reddening law. Thus, these diagrams can distinguish between foreground stars and cluster stars. There remains, of course, some ambiguity concerning the stars which lie near to the front edge of the cluster.

Figures 9a and 9b show the $(v-i, B-V)$ and $(v-r, B-V)$ TCDs, respectively for the probable cluster members obtained from the P–Q diagram (the $v-r$ and $v-i$ colours are in the instrumental system). The dashed line shows the loci of the main-sequence stars reddened by the normal extinction law. These lines have been taken from the ensuing figures 10a and 10b. The loci of probable

Table 1a. Magnitudes and colours of the stars in the field of NGC 3603.

No	X	Y	V	$U-B$	$B-V$	$E(B-V)$	Radius ($''$)	Remark
1	9.89	192.48	16.478	0.063	0.723	0.88	73.07	
2	9.94	92.50	13.920	0.127	0.358	0.41	96.15	
3	10.60	245.68	17.878	*	0.956	*	66.80	
4	11.35	416.91	16.983	*	1.131	*	86.97	M
5	12.15	270.64	16.979	*	1.631	*	65.46	M
6	13.90	378.47	16.949	*	1.181	*	77.16	M
7	16.81	371.90	15.979	0.255	0.610	0.68	74.83	
8	22.24	481.77	16.492	*	0.804	*	102.68	
9	24.18	114.58	16.333	0.146	0.716	0.85	86.11	
10	26.69	190.59	17.463	*	1.086	*	67.52	
11	35.38	227.91	17.500	*	0.974	*	58.85	
12	35.71	246.27	17.070	*	2.025	*	57.09	
13	37.79	363.05	17.642	*	0.918	*	66.07	
14	38.36	268.80	17.295	*	0.771	*	55.25	
15	39.38	11.55	17.740	*	1.476	*	115.09	
16	40.56	278.08	14.010	−0.069	1.216	1.55	54.45	m, M
17	43.52	219.23	16.776	*	1.393	*	56.93	M
18	44.47	396.58	15.789	*	2.123	*	72.06	
19	49.24	146.26	15.590	0.041	1.383	1.72	70.48	M
20	53.81	112.22	17.113	*	1.362	*	79.10	M
21	54.15	228.40	17.582	*	1.599	*	51.82	M
22	54.19	20.49	17.447	*	1.025	*	109.33	
23	59.45	368.64	16.268	*	0.831	*	60.50	
24:	60.65	182.48	16.270	0.029	1.285	1.61	57.95	
25	63.82	65.83	17.387	*	1.472	*	91.95	M
26	66.06	281.47	15.264	0.258	0.839	0.97	44.62	
27	67.25	206.81	15.400	0.070	0.644	0.78	50.60	Hα
28	68.47	375.41	15.372	*	1.588	*	59.58	
29	70.44	200.23	17.282	*	1.147	*	50.87	M
30	72.31	475.26	17.126	*	0.954	*	90.05	
31	72.67	72.47	17.811	*	0.644	*	88.02	M
32	73.48	43.64	16.665	*	1.447	*	97.92	
33	73.93	204.59	14.459	−0.161	1.096	1.43	48.80	m, M
34	75.19	306.44	16.933	*	1.595	*	43.15	M
35	76.97	510.06	16.418	*	1.191	*	101.52	M
36	77.58	87.61	17.280	*	1.362	*	81.92	M
37	80.50	175.95	17.540	*	1.138	*	53.66	M
38	82.50	199.86	17.320	−0.322	1.126	1.52	47.07	M
39:	86.95	221.42	16.307	0.014	1.079	1.35	41.12	
40	91.57	357.39	17.232	*	1.049	*	48.22	M
41:	92.52	208.48	15.679	−0.139	1.097	1.42	41.93	
42	92.65	382.93	15.099	0.396	0.869	0.96	55.37	
43	93.00	332.67	16.498	*	1.422	*	41.59	M
44	95.20	93.21	16.389	*	1.363	*	76.82	M
45	98.66	169.00	15.910	−0.027	1.123	1.42	50.88	m, M, Hα
46	100.38	422.44	18.414	*	0.959	*	66.73	
47:	105.97	203.21	15.760	0.351	0.951	1.08	39.15	
48	106.26	9.55	15.368	−0.024	0.632	0.80	105.94	
49	106.41	220.49	16.712	*	0.825	*	34.81	
50	107.11	162.66	14.889	−0.110	1.214	1.56	50.93	m, M

Table 1a. (Continued)

No	X	Y	V	$U-B$	$B-V$	$E(B-V)$	Radius ($''$)	Remark
51	107.20	290.91	15.466	−0.029	1.191	1.50	29.43	m, M
52	110.47	307.11	16.254	*	1.801	*	30.56	
53	110.87	258.46	17.622	*	1.367	*	27.40	
54	113.28	152.45	17.528	*	1.112	*	53.06	
55	114.66	145.38	16.510	*	1.241	*	55.22	
56	115.11	272.09	16.631	0.135	0.874	1.05	25.31	M
57	115.37	188.70	13.967	−0.149	1.069	1.39	40.81	m, M
58	116.81	251.38	14.640	−0.084	1.211	1.55	25.81	m, M
59	118.14	277.80	16.751	*	1.248	*	24.27	M
60	119.30	51.74	17.011	*	2.221	*	88.73	
61	120.13	227.95	12.701	−0.170	1.137	1.48	28.76	M
62	122.63	185.91	15.539	0.211	0.608	0.69	40.02	
63:	125.25	333.80	15.734	0.056	1.384	1.72	32.49	
64	125.69	239.77	12.632	−0.091	1.195	1.53	24.43	M
65	126.32	80.35	17.287	*	1.458	*	77.24	M
66	128.08	128.31	17.783	*	0.953	*	59.22	
67	128.57	144.41	16.013	0.064	1.273	1.58	53.29	m, M
68:	129.05	255.64	17.408	*	1.377	*	20.76	
69	129.43	101.89	15.265	0.059	1.325	1.64	68.84	m, M
70	130.83	260.07	17.111	*	1.418	*	19.64	
71	133.88	25.34	17.826	*	1.442	*	97.48	
72	134.35	172.04	17.390	*	1.292	*	42.50	M
73	136.04	84.64	17.411	−0.542	1.388	1.73	74.68	M
74	136.09	191.51	13.614	−0.250	1.010	1.35	35.42	M
75	136.93	254.96	16.945	*	1.202	*	17.92	M
76	136.95	215.43	17.497	*	1.168	*	27.41	M
77	138.32	132.17	17.254	*	1.250	*	56.53	M
78	138.90	301.26	17.190	*	1.250	*	19.91	
79:	139.02	268.44	14.432	−0.093	1.109	1.42	16.01	
80	139.37	279.16	17.455	*	1.272	*	16.16	M
81	139.68	210.05	16.197	−0.071	1.019	1.30	28.50	m, M
82:	140.97	259.76	16.649	*	1.172	*	15.84	
83	144.56	277.34	15.773	0.049	1.119	1.39	14.04	PMS
84	145.02	426.84	17.285	*	0.907	*	62.29	
85	145.74	238.49	17.393	*	1.655	*	18.42	
86	146.69	291.24	17.360	*	1.272	*	15.20	M
87	147.10	244.99	16.409	*	1.191	*	16.36	M
88	147.36	508.17	17.535	*	1.113	*	93.37	M
89	149.38	313.48	16.055	−0.133	1.110	1.44	20.42	m, M
90	149.48	254.42	15.102	−0.194	1.116	1.47	13.54	m, M
91	154.44	316.20	15.101	−0.177	1.107	1.45	20.25	m, M
92	155.59	219.29	15.603	−0.138	1.122	1.46	22.30	m, M
93:	156.26	280.36	16.493	*	1.191	*	9.95	
94	156.38	326.51	16.677	−0.134	1.144	1.48	23.53	M
95	158.11	248.87	13.235	−0.208	1.049	1.39	12.14	m, M
96	158.60	406.46	16.852	*	0.892	*	53.48	
97	159.81	155.98	17.414	*	1.256	*	45.54	M
98	159.99	299.39	16.029	0.167	1.444	1.76	13.54	m, M, Hα
99	160.19	224.67	14.077	−0.207	1.067	1.41	19.65	m, M
100	160.68	261.54	13.463	−0.261	1.025	1.37	8.39	m

Table 1a. (Continued)

No	X	Y	V	$U-B$	$B-V$	$E(B-V)$	Radius ($''$)	Remark
101:	161.85	334.92	15.327	0.025	1.070	1.34	25.92	
102:	161.98	283.87	16.103	−0.105	1.190	1.53	8.63	
103	162.02	189.81	14.763	−0.168	1.096	1.43	32.43	m, M
104	162.32	206.71	17.430	*	1.132	*	26.01	M
105	162.44	311.81	18.027	*	1.109	*	17.33	M
106:	163.00	238.57	14.745	−0.252	0.934	1.26	14.28	
107	163.43	164.55	15.782	−0.093	1.142	1.47	42.01	m, M
108	163.58	269.54	13.950	−0.211	0.999	1.33	6.43	a
109	165.24	273.79	13.342	−0.244	1.015	1.36	5.86	m, M
110	166.65	23.74	15.106	0.179	0.801	0.94	96.57	
111	167.09	300.02	17.172	*	1.161	*	12.39	M
112:	167.54	258.91	14.694	0.043	0.923	1.14	6.77	
113	168.33	430.44	17.654	*	1.241	*	62.35	M
114	168.72	334.04	17.335	*	0.864	*	24.98	
115	169.29	402.24	17.006	*	1.441	*	51.36	M
116	170.49	173.63	17.137	*	1.336	*	38.15	
117:	171.25	275.45	13.607	−0.146	0.933	1.22	3.83	
118:	171.35	234.33	14.450	−0.135	1.112	1.44	14.70	
119:	174.39	257.26	13.555	−0.073	1.001	1.28	5.79	
120:	175.56	250.46	14.302	−0.226	0.961	1.28	8.19	
121	176.16	355.57	12.557	−0.104	0.130	0.20	33.02	
122	176.74	316.89	17.628	*	1.373	*	17.94	
123	179.55	297.64	16.995	*	1.092	*	10.39	a
124:	180.96	242.51	13.600	−0.196	0.914	1.21	11.12	
125:	181.42	213.86	13.223	−0.183	1.119	1.47	22.29	
126	184.16	195.44	14.738	−0.166	1.112	1.45	29.51	m, M
127	185.77	18.42	15.492	0.124	0.808	0.97	98.53	
128:	186.29	284.48	12.811	−0.225	1.004	1.34	5.80	
129	186.91	54.93	17.606	*	1.391	*	84.31	M
130	187.19	202.83	17.688	*	1.266	*	26.73	M
131:	187.96	273.83	12.069	−0.198	0.867	1.15	3.30	
132:	188.49	247.24	15.025	−0.226	1.027	1.37	9.84	
133:	188.58	430.56	13.989	0.723	1.104	1.14	62.32	
134:	188.72	326.28	14.543	−0.182	1.046	1.37	21.82	
135:	189.01	257.13	13.181	0.289	0.564	0.61	6.45	
136:	189.69	265.85	12.662	−0.180	0.940	1.24	4.28	
137:	189.76	241.02	15.810	−0.040	1.107	1.40	12.30	
138	189.88	493.67	17.091	*	0.949	*	86.93	
139	191.53	42.30	16.127	0.140	1.381	1.69	89.31	m, M
140	191.56	251.09	15.195	−0.204	0.963	1.28	8.98	a
141:	191.92	287.84	15.865	−0.310	0.491	0.72	8.05	
142	192.27	166.39	17.445	*	1.310	*	41.08	
143	192.77	302.57	17.834	*	1.656	*	13.28	
144	193.02	313.47	17.824	*	1.043	*	17.32	a
145	193.46	28.29	12.720	−0.180	0.663	0.89	94.80	
146	193.51	58.98	16.983	*	0.929	*	82.86	
147:	193.98	231.26	14.628	−0.196	1.081	1.42	16.43	
148	195.35	367.53	16.699	*	1.148	*	38.12	M
149	195.52	310.02	17.544	*	1.300	*	16.38	
150:	196.37	275.31	13.833	−0.153	0.773	1.02	6.60	

Table 1a. (Continued)

No	X	Y	V	$U-B$	$B-V$	$E(B-V)$	Radius ($''$)	Remark
151:	197.05	248.09	15.907	−0.103	1.123	1.45	11.14	
152	197.07	48.50	17.292	*	1.346	*	87.03	M
153	197.36	291.02	17.031	*	0.994	*	10.34	a
154	197.48	152.36	17.692	*	1.450	*	46.77	
155	199.56	283.55	15.964	−0.144	0.927	1.21	9.06	
156:	200.45	258.95	13.975	−0.223	0.781	1.05	9.26	
157	200.78	217.86	12.664	−0.138	1.146	1.49	22.25	M
158	203.12	393.60	15.998	−0.023	1.106	1.40	48.66	m, M
159	203.25	50.65	15.802	0.024	1.364	1.71	86.41	m, M
160	203.45	166.70	17.902	*	1.299	*	41.69	M
161:	205.25	271.44	16.239	0.132	1.070	1.30	9.85	
162	205.26	279.54	16.435	−0.228	1.109	1.47	10.40	Hα
163	207.73	255.20	13.579	−0.187	1.091	1.43	12.45	m, M
164	208.59	362.81	13.380	0.042	0.513	0.63	37.50	
165	209.02	280.86	16.456	*	1.061	*	11.95	a
166	209.08	235.15	14.218	−0.154	1.097	1.43	18.00	m, M
167	210.54	294.87	15.083	−0.135	1.043	1.36	15.12	m, M
168:	211.18	285.88	14.901	−0.092	1.038	1.33	13.47	
169	211.28	381.86	16.659	*	1.037	*	44.92	M
170	212.59	275.20	16.760	*	1.119	*	12.82	M
171	212.79	222.60	17.530	*	1.354	*	22.80	M
172	212.79	173.49	15.500	−0.050	1.289	1.64	40.12	m, M
173	217.77	403.23	15.009	−0.050	1.173	1.49	53.63	m, M
174:	218.55	244.88	16.053	0.223	0.912	1.07	18.16	
175	218.59	277.26	14.660	−0.086	1.120	1.43	15.25	m, M
176	219.84	212.80	17.629	*	1.277	*	27.51	M
177	221.10	326.90	14.975	−0.240	1.040	1.39	27.06	m, M
178:	224.29	138.45	14.995	0.195	1.483	1.80	54.50	
179	224.32	312.68	18.231	*	1.270	*	23.73	M
180	224.70	283.69	16.343	0.278	1.138	1.34	18.12	PMS, M
181	224.93	269.79	15.940	0.030	1.158	1.44	17.53	m, M
182	225.42	457.25	17.172	*	0.805	*	74.77	
183	226.94	294.45	17.604	*	1.220	*	20.46	M
184	227.37	399.77	16.100	0.303	0.898	1.02	53.51	M
185	228.41	228.63	16.362	*	0.996	*	25.09	
186	228.93	486.74	14.077	−0.090	1.203	1.54	86.28	m, M
187	229.82	62.03	16.694	*	1.422	*	83.78	M
188:	232.60	301.27	14.522	0.067	0.725	0.89	23.67	
189	233.17	198.84	17.012	*	1.316	*	34.96	M
190	234.24	258.03	12.201	0.120	1.424	1.61	21.75	M
191	235.11	186.55	14.778	0.072	1.464	1.82	39.33	m, M
192	236.40	371.91	17.748	*	0.823	*	45.08	
193	237.14	463.89	18.030	*	0.968	*	78.46	
194	240.62	493.26	15.931	0.142	0.817	0.98	89.85	
195	249.35	119.57	15.264	0.138	0.630	0.74	64.95	
196	250.34	467.69	15.607	0.110	1.356	1.67	81.47	m, M
197	253.26	482.47	15.240	0.062	0.645	0.79	87.28	
198	256.40	272.88	17.770	*	1.214	*	29.80	
199	259.27	30.09	18.020	*	1.055	*	98.91	
200	259.44	238.32	17.224	*	1.062	*	33.50	

Table 1a. (Continued)

No	X	Y	V	$U-B$	$B-V$	$E(B-V)$	Radius ($''$)	Remark
201	260.47	354.70	17.267	*	1.363	*	45.28	M
202:	264.64	5.13	14.845	−0.365	2.012	2.66	108.82	
203	273.74	238.33	16.536	*	1.068	*	38.72	
204	276.08	385.86	15.183	0.032	1.375	1.72	58.40	m, M
205	277.38	335.69	14.763	0.095	0.682	0.82	45.59	
206	277.39	373.53	16.203	−0.022	1.446	1.83	55.15	M
207	279.16	394.93	17.235	*	1.189	*	61.90	
208	282.51	306.73	16.973	*	1.744	*	42.34	M
209	283.39	159.49	16.416	*	1.066	*	59.31	
210	284.52	64.58	16.905	*	1.568	*	90.23	M
211	289.39	495.53	17.225	*	0.889	*	97.41	
212	293.13	130.51	15.911	0.122	1.456	1.79	70.35	m, M
213	295.16	73.41	16.212	*	1.516	*	89.19	M
214	307.58	314.41	16.667	*	1.405	*	52.56	M

Remarks:
(i) Star number marked with ':' has not been included in the analysis.
(ii) Stars marked 'm' are probable members from P–Q diagram.
(iii) Stars marked 'M' are probable members from $V-X/B-V$ diagrams.
(iv) The stars shown by diamond symbol in figure 10 are marked as 'a'.

cluster members can also be represented by a straight line having a different slope, indicating that the cluster region has anomalous reddening. Figures 10a and 10b show the $(v-i, B-V)$ and $(v-r, B-V)$ TCDs, respectively, for all of the stars measured. An inspection of these TCDs shows three distinct groups of objects:

a) Stars which follow the dashed lines (open circles). They are foreground stars which are reddened according to the normal extinction law $E(V-I)/E(B-V) = 1.25$.

b) Cluster stars which fall consistently below the dashed lines in both TCDs (filled circles). Their locations can also be represented by straight lines having a tilt steeper than the dashed lines. The membership of the stars near to the point of intersection is decided on the basis of their distance from the cluster center and the amount of reddening. Stars within a radius of $60''$ and having $E(B-V) \geq 1.00$ mag are considered to be probable members.

c) Objects located further left of group (b) in both TCDs (open diamonds). The explanation of this anomaly includes i) much more anomalous reddening law, ii) excess of radiation due to circumstellar dust, and iii) a close-by red companion (Chini, Wargau 1990). Since none of the stars in this group show Hα emission, point (ii) can probably be excluded. Because all of these stars are located in the central region, we take stars in group (c) as cluster members.

To derive the value of $R_{\rm cluster}$ (ratio of total to selective extinction of the intra-cluster medium) we use the following approximate relation (cf. Neckel, Chini 1981):

$$R_{\rm cluster} = \frac{m_{\rm cluster}}{m_{\rm normal}} \times R_{\rm normal}$$

Here, $m_{\rm cluster}$ and $m_{\rm normal}$ are the slopes of the lines followed by cluster stars and field stars, respectively, and $R_{\rm normal} = 3.1$. For stars having $V \leq 17.0$, both the $(v-r, B-V)$ and $(v-i, B-V)$ TCDs give a value of $R_{\rm cluster} = 4.3 \pm 0.2$ (s.e.), whereas the whole sample gives a value of $R_{\rm cluster} = 4.1 \pm 0.2$ (s.e.).

Recently, Eisenhauer et al. (1998) have reported JHK CCD photometry for the cluster. There are 11 common stars in the data of Eisenhauer et al. and the present work, whereas the data of Melnick et al. have nine common stars. By combining these three data sets we derived the $(V-J), (V-H), (V-K)$ values for 15 stars. These stars have been used to generate $(V-J, B-V), (V-H, B-V), (V-K, B-V)$ TCDs; the TCDs are shown in figure 11 . The probable cluster members of these diagrams give $R_{\rm cluster} = 5.2 \pm 1.0$, 4.8 ± 0.8, and 4.2 ± 0.7, respectively. Thus, the near-IR data also support anomalous reddening in the cluster region.

However, we prefer $R_{\rm cluster} = 4.3 \pm 0.2$ obtained from optical observations having $V \leq 17.0$, because of the smaller error in the sample; also this value is used in subsequent sections.

Table 1b. The instrumental magnitude and colours of the stars.

No	X	Y	$v-r$	$v-i$	Hα	Continuum
1	9.89	192.48	1.057	0.576	24.585	19.886
2	9.94	92.50	0.844	−0.071	21.723	17.551
3	10.60	245.68	1.313	0.796	*	*
4	11.35	416.91	1.485	1.335	*	19.914
5	12.15	270.64	1.755	2.037	*	19.475
6	13.90	378.47	1.428	1.192	23.384	19.877
7	16.81	371.90	1.010	0.266	23.730	19.335
8	22.24	481.77	1.193	0.672	23.910	19.600
9	24.18	114.58	1.005	0.285	23.875	19.774
10	26.69	190.59	1.204	0.615	*	*
11	35.38	227.91	1.123	0.494	*	*
12	35.71	246.27	1.664	1.686	24.738	19.694
13	37.79	363.05	1.173	0.629	*	*
14	38.36	268.80	1.312	0.706	*	*
15	39.38	11.55	1.563	1.402	*	20.678
16	40.56	278.08	1.500	1.377	20.854	16.864
17	43.52	219.23	1.572	1.674	*	19.474
18	44.47	396.58	1.903	2.068	22.264	18.207
19	49.24	146.26	1.558	1.528	22.604	18.394
20	53.81	112.22	1.583	1.593	*	19.881
21	54.15	228.40	1.602	1.748	*	20.184
22	54.19	20.49	1.219	0.630	*	20.468
23	59.45	368.64	1.130	0.484	23.095	19.575
24:	60.65	182.48	1.468	1.319	22.718	19.375
25	63.82	65.83	1.654	1.667	*	20.035
26	66.06	281.47	1.065	0.384	22.825	18.578
27	67.25	206.81	1.086	0.346	22.031	18.820
28	68.47	375.41	1.564	1.380	22.232	18.147
29	70.44	200.23	1.550	1.310	*	20.214
30	72.31	475.26	1.189	0.622	*	*
31	72.67	72.47	1.687	1.317	*	*
32	73.48	43.64	1.558	1.492	23.737	19.598
33	73.93	204.59	1.368	1.118	21.440	17.489
34	75.19	306.44	1.683	1.776	24.158	19.573
35	76.97	510.06	1.482	1.296	*	19.394
36	77.58	87.61	1.607	1.614	23.992	*
37	80.50	175.95	1.364	1.284	*	*
38	82.50	199.86	1.503	1.172	*	20.338
39:	86.95	221.42	1.594	1.351	*	19.333
40	91.57	357.39	1.370	1.254	*	*
41:	92.52	208.48	1.537	1.111	21.363	18.744
42	92.65	382.93	1.137	0.500	22.297	18.388
43	93.00	332.67	1.565	1.608	*	19.295
44	95.20	93.21	1.566	1.538	23.301	19.314
45	98.66	169.00	1.390	1.131	22.302	18.945
46	100.38	422.44	1.247	0.767	*	*
47:	105.97	203.21	1.231	0.753	22.267	19.007
48	106.26	9.55	0.984	0.229	22.929	18.825
49	106.41	220.49	1.111	0.687	*	19.959
50	107.11	162.66	1.431	1.264	21.920	17.841

Table 1b. (Continued)

No	X	Y	$v-r$	$v-i$	Hα	Continuum
51	107.20	290.91	1.419	1.258	22.681	18.382
52	110.47	307.11	1.695	1.628	22.796	18.957
53	110.87	258.46	1.384	1.223	*	*
54	113.28	152.45	1.452	1.247	*	*
55	114.66	145.38	1.386	1.193	23.631	19.472
56	115.11	272.09	1.148	0.576	*	19.822
57	115.37	188.70	1.344	1.080	21.131	17.012
58	116.81	251.38	1.440	1.288	21.661	17.564
59	118.14	277.80	1.418	1.250	23.829	19.707
60	119.30	51.74	2.012	2.320	23.566	19.410
61	120.13	227.95	*	1.125	19.763	15.702
62	122.63	185.91	0.968	0.301	23.194	19.038
63:	125.25	333.80	1.673	1.610	22.340	18.556
64	125.69	239.77	*	1.303	19.482	15.537
65	126.32	80.35	1.581	1.561	*	*
66	128.08	128.31	1.196	0.569	*	*
67	128.57	144.41	1.533	1.454	22.749	18.846
68:	129.05	255.64	1.369	1.361	*	*
69	129.43	101.89	1.497	1.405	22.390	18.140
70	130.83	260.07	1.322	1.339	*	19.962
71	133.88	25.34	1.471	1.426	*	*
72	134.35	172.04	1.460	1.377	*	*
73	136.04	84.64	1.547	1.510	*	20.254
74	136.09	191.51	1.298	0.958	20.803	16.694
75	136.93	254.96	1.291	1.270	*	19.759
76	136.95	215.43	1.089	0.935	*	*
77	138.32	132.17	1.489	1.411	*	*
78	138.90	301.26	1.276	0.768	*	*
79:	139.02	268.44	1.378	1.153	21.571	17.429
80	139.37	279.16	1.515	1.446	*	*
81	139.68	210.05	1.218	0.847	23.328	19.268
82:	140.97	259.76	1.337	1.551	23.920	*
83	144.56	277.34	1.412	1.231	22.927	18.793
84	145.02	426.84	1.250	0.706	*	20.340
85	145.74	238.49	1.155	1.319	*	*
86	146.69	291.24	1.445	1.189	*	*
87	147.10	244.99	1.330	1.176	23.734	19.460
88	147.36	508.17	1.390	1.117	*	*
89	149.38	313.48	1.330	0.989	23.785	19.149
90	149.48	254.42	1.348	1.144	22.344	18.123
91	154.44	316.20	1.344	1.063	22.506	18.082
92	155.59	219.29	1.273	0.913	23.037	18.720
93:	156.26	280.36	1.623	1.606	23.762	19.461
94	156.38	326.51	1.402	1.192	*	19.782
95	158.11	248.87	1.352	1.062	20.289	16.293
96	158.60	406.46	1.202	0.658	*	18.862
97	159.81	155.98	1.439	1.232	*	*
98	159.99	299.39	1.716	1.835	21.745	18.805
99	160.19	224.67	1.301	0.977	21.290	17.181
100	160.68	261.54	1.413	1.140	20.578	16.486

Table 1b. (Continued)

No	X	Y	$v-r$	$v-i$	Hα	Continuum
101:	161.85	334.92	1.390	1.121	21.396	18.435
102:	161.98	283.87	1.535	1.669	23.208	18.989
103	162.02	189.81	1.319	1.034	21.953	17.819
104	162.32	206.71	1.266	0.962	*	20.618
105	162.44	311.81	1.443	1.162	*	*
106:	163.00	238.57	1.318	1.068	21.982	17.839
107	163.43	164.55	1.362	1.127	22.940	18.845
108	163.58	269.54	1.356	1.176	21.155	17.005
109	165.24	273.79	1.344	1.046	20.499	16.402
110	166.65	23.74	1.053	0.356	22.603	18.454
111	167.09	300.02	1.355	1.138	*	*
112:	167.54	258.91	1.464	1.362	21.897	17.726
113	168.33	430.44	1.540	1.505	*	*
114	168.72	334.04	1.371	0.713	*	*
115	169.29	402.24	1.624	1.671	24.142	19.793
116	170.49	173.63	1.437	1.263	*	19.973
117:	171.25	275.45	1.375	1.136	20.906	16.826
118:	171.35	234.33	1.348	1.101	21.689	17.563
119:	174.39	257.26	1.465	1.264	21.916	16.832
120:	175.56	250.46	1.325	1.160	21.475	17.358
121	176.16	355.57	0.664	−0.424	20.510	16.387
122	176.74	316.89	1.170	1.016	*	*
123	179.55	297.64	1.575	1.533	*	*
124:	180.96	242.51	1.334	1.228	20.811	16.730
125:	181.42	213.86	1.350	1.102	20.327	16.301
126	184.16	195.44	1.366	1.111	21.880	17.750
127	185.77	18.42	1.065	0.329	23.023	18.910
128:	186.29	284.48	1.373	1.014	20.125	16.025
129	186.91	54.93	1.561	1.547	*	*
130	187.19	202.83	1.529	1.426	*	*
131:	187.96	273.83	*	1.054	19.254	15.201
132:	188.49	247.24	1.297	1.134	22.313	18.155
133:	188.58	430.56	1.250	0.753	21.206	17.116
134:	188.72	326.28	1.338	1.048	21.751	17.598
135:	189.01	257.13	1.318	1.086	20.766	16.489
136:	189.69	265.85	1.469	1.306	20.052	15.923
137:	189.76	241.02	1.303	1.287	23.035	18.893
138	189.88	493.67	1.195	0.572	*	*
139	191.53	42.30	1.531	1.435	22.988	19.014
140	191.56	251.09	1.396	1.186	22.388	18.255
141:	191.92	287.84	1.532	1.480	*	18.770
142	192.27	166.39	1.261	0.865	*	20.436
143	192.77	302.57	1.387	1.583	*	*
144	193.02	313.47	1.327	1.266	*	*
145	193.46	28.29	1.081	0.477	20.090	16.082
146	193.51	58.98	1.260	0.816	*	20.026
147:	193.98	231.26	1.320	1.018	21.795	17.690
148	195.35	367.53	1.401	1.133	24.232	19.719
149	195.52	310.02	1.327	1.133	*	*
150:	196.37	275.31	1.482	1.174	21.085	16.942

Table 1b. (Continued)

No	X	Y	$v-r$	$v-i$	Hα	Continuum
151:	197.05	248.09	1.345	1.299	23.352	18.974
152	197.07	48.50	1.479	1.364	*	*
153	197.36	291.02	1.487	1.309	*	20.237
154	197.48	152.36	1.495	1.402	*	*
155	199.56	283.55	1.449	1.261	*	19.015
156:	200.45	258.95	1.325	1.279	21.158	17.015
157	200.78	217.86	*	1.113	19.737	15.687
158	203.12	393.60	1.425	1.195	22.956	18.940
159	203.25	50.65	1.516	1.451	22.767	18.723
160	203.45	166.70	1.524	1.416	*	*
161:	205.25	271.44	1.780	1.751	23.098	19.095
162	205.26	279.54	1.459	1.104	22.127	19.432
163	207.73	255.20	1.357	1.083	20.722	16.611
164	208.59	362.81	0.919	0.097	21.048	16.897
165	209.02	280.86	1.540	1.236	*	19.549
166	209.08	235.15	1.294	1.025	21.373	17.267
167	210.54	294.87	1.362	0.986	21.919	18.165
168:	211.18	285.88	1.389	1.032	21.154	18.051
169	211.28	381.86	1.341	1.027	*	19.641
170	212.59	275.20	1.421	1.194	*	19.854
171	212.79	222.60	1.540	1.413	*	*
172	212.79	173.49	1.483	1.351	22.524	18.434
173	217.77	403.23	1.424	1.219	22.028	17.962
174:	218.55	244.88	1.340	1.470	23.096	19.111
175	218.59	277.26	1.375	1.077	21.658	17.702
176	219.84	212.80	1.345	1.319	*	*
177	221.10	326.90	1.312	0.985	22.197	18.058
178:	224.29	138.45	1.637	1.528	21.992	17.824
179	224.32	312.68	1.514	1.459	*	*
180	224.70	283.69	1.443	1.143	*	19.341
181	224.93	269.79	1.340	1.173	23.233	18.948
182	225.42	457.25	1.230	0.792	*	*
183	226.94	294.45	1.953	1.333	*	*
184	227.37	399.77	1.174	0.572	23.583	19.363
185	228.41	228.63	1.104	0.521	23.567	19.613
186	228.93	486.74	1.436	1.273	21.139	17.016
187	229.82	62.03	1.549	1.486	23.767	19.583
188:	232.60	301.27	1.001	0.566	22.050	17.982
189	233.17	198.84	1.563	1.553	*	19.796
190	234.24	258.03	*	1.573	19.042	14.990
191	235.11	186.55	1.613	1.616	21.659	17.539
192	236.40	371.91	1.177	0.485	*	*
193	237.14	463.89	1.307	0.830	*	*
194	240.62	493.26	1.092	0.440	23.086	19.324
195	249.35	119.57	0.983	0.235	22.889	18.697
196	250.34	467.69	1.564	1.551	22.601	18.447
197	253.26	482.47	1.016	0.322	22.817	18.638
198	256.40	272.88	1.237	0.792	*	*
199	259.27	30.09	1.333	0.944	*	*
200	259.44	238.32	1.212	0.736	*	*

Table 1b. (Continued)

No	X	Y	$v-r$	$v-i$	Hα	Continuum
201	260.47	354.70	1.618	1.606	*	*
202:	264.64	5.13	1.941	2.090	21.408	17.321
203	273.74	238.33	1.204	0.596	23.825	*
204	276.08	385.86	1.617	1.612	22.104	17.955
205	277.38	335.69	0.998	0.236	22.242	18.179
206	277.39	373.53	1.658	1.741	23.115	18.902
207	279.16	394.93	1.291	0.840	*	20.248
208	282.51	306.73	1.906	2.227	23.887	19.431
209	283.39	159.49	1.310	0.950	23.708	19.529
210	284.52	64.58	1.694	1.800	23.587	19.511
211	289.39	495.53	1.096	0.452	*	*
212	293.13	130.51	1.616	1.646	22.880	18.705
213	295.16	73.41	1.647	1.669	22.984	19.051
214	307.58	314.41	1.706	1.773	23.294	19.420

Note. Star number marked with ':' has not been included in the analysis.

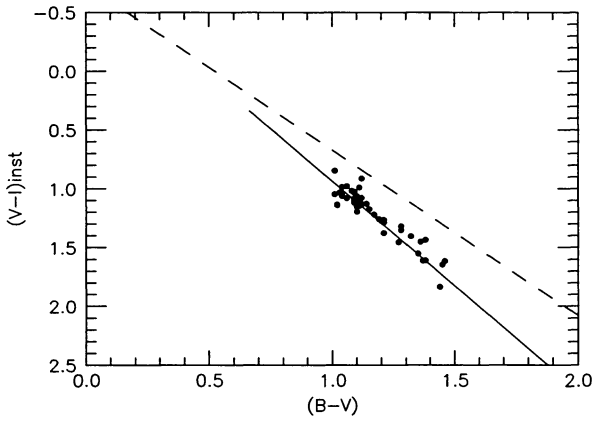

Fig. 9a. $(v-i, B-V)$ diagram for the probable cluster members, as determined from the P–Q diagram. The solid line follows the distribution of probable cluster members and the dashed line shows the loci of field stars reddened by the normal reddening law. See the text.

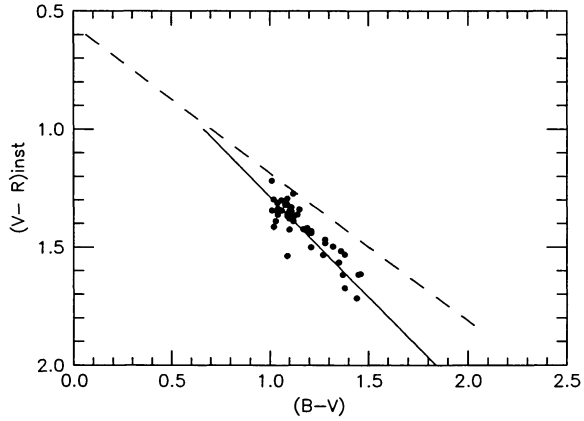

Fig. 9b. $(v-r, B-V)$ diagram for the probable cluster members, as determined from the P–Q diagram. The lines are the same as in figure 9a.

5.2. *Variable Extinction Analysis*

The variable extinction method can also be applied to derive the R value. The probable main-sequence stars, selected from the P–Q diagram (cf section 4), were used for the ZAMS fitting version of the method (Turner 1976). The apparent distance moduli, $V-M_V$ were derived by using the ZAMS given by Schmidt-Kaler (1982). The resultant variable extinction diagram is shown in figure 12. Although the scatter is relatively large, most of the stars follow a trend and a least-squares fit to all points gives $R_{\rm cluster} = 3.0 \pm 0.6$, whereas the data in the range $1.30 \leq E(B-V) \leq 1.75$ give a value of $R_{\rm cluster} = 3.8 \pm 0.8$.

The $V-M_V$ and $E(B-V)$ for nine stars have also been obtained from spectral classification (Moffat 1983) and using the intrinsic colours and ZAMS given by Schmidt-Kaler (1982). These are also plotted in figure 12 by diamonds, which seem to follow the trend, though we did not include them in the above-mentioned least-squares fits.

6. Colour Magnitude Diagram of the Cluster

The above discussions indicate an abnormal reddening law inside the cluster NGC 3603. The absorption for foreground stars having $E(B-V) < 1.1$ was obtained

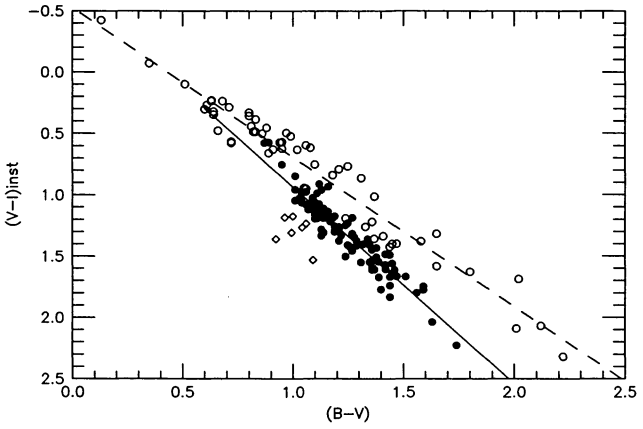

Fig. 10a. $(v-i, B-V)$ diagram for all stars in the cluster region. The solid and dashed lines follow the distribution of cluster stars and that of field stars, respectively.

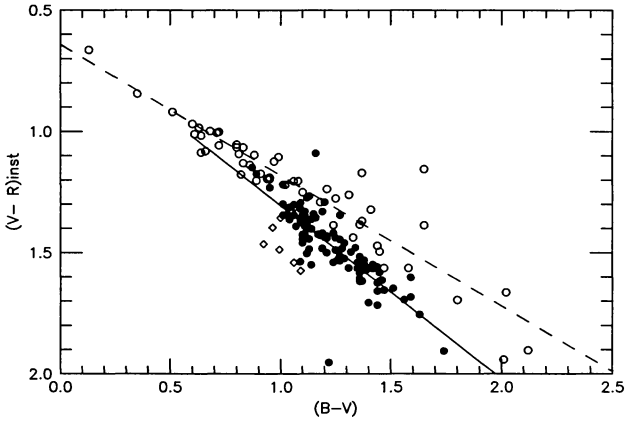

Fig. 10b. $(v-r, B-V)$ diagram for all stars in the cluster region. The lines are the same as in figure 10a.

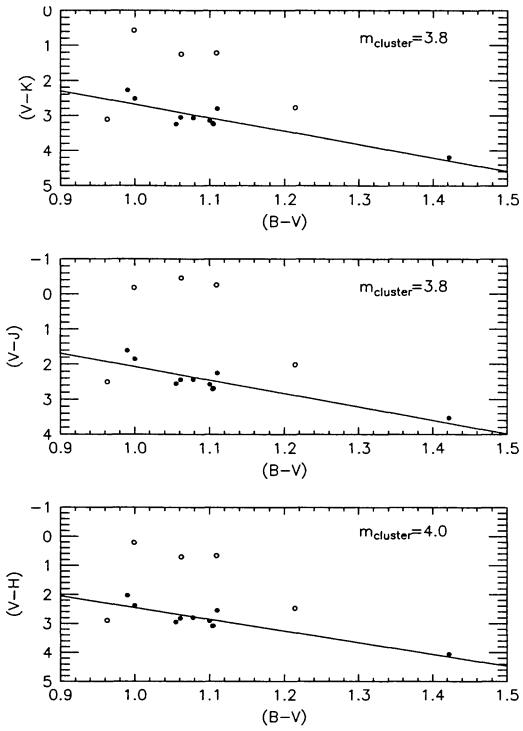

Fig. 11. $(V-K, B-V), (V-J, B-V), (V-H, B-V)$ diagrams. The probable cluster members are shown by filled circles.

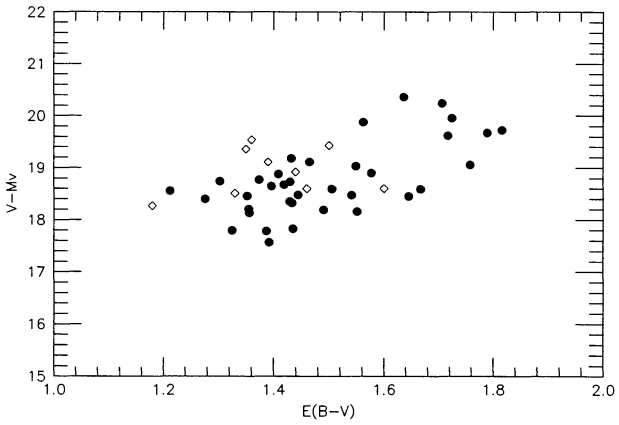

Fig. 12. Variable extinction diagram for NGC 3603. The $V-M_V$ and $E(B-V)$ for nine stars were also obtained from the spectral classification (see text); these are indicated by diamonds.

from the relation $A_V = 3.1 \times E(B-V)$, whereas for the absorption for probable cluster stars [having $E(B-V) > 1.1$] we used the relation $A_V = 3.1 \times 1.1 + 4.3\,[E(B-V) - 1.1]$. The $E(B-V)$ value was derived for individual stars using the Q method (Johnson, Morgan 1953). The $E(B-V)$ has also been derived for nine stars using the spectral classifications given by Moffat (1983) and the intrinsic colours given by Schmidt-Kaler (1982). A comparison, in the sense $E(B-V)_{Q\text{method}} - E(B-V)_{\text{MK}}$, gives a value of ~ 0.03. This correction has been applied to the $E(B-V)_{Q\text{method}}$ values.

Figures 13a and 13b show the $(V, B-V)$ and $(V, U-B)$ colour–magnitude diagrams (CMDs) of the cluster, respectively, together with the theoretical isochrones of Maeder and Meynet (1987). To convert these theoretical isochrones to the observational plane, we adopted the bolometric corrections and T_{eff}–$(B-V)_0$ relation from Sagar et al. (1986). These CMDs give distance moduli of $(m-M)_0 = 13.9$ and 14.1, respectively. We use the mean value of the distance modulus $(m-M)_0 = 14.0$ for further discussions. The distance modulus corresponds to a distance of 6.3 ± 0.6 kpc, which is in good agreement with

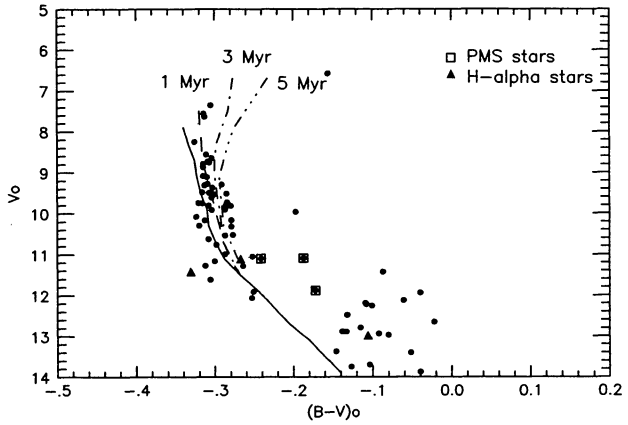

Fig. 13a. (V, $B-V$) colour–magnitude diagram of NGC 3603.

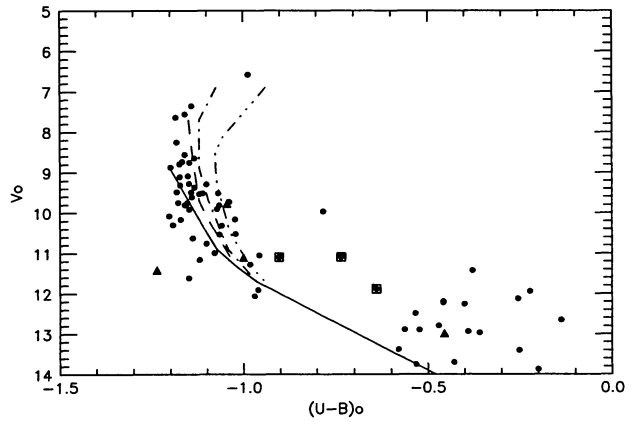

Fig. 13b. (V, $U-B$) colour–magnitude diagram of NGC 3603. The curves and symbols are the same as in figure 13a.

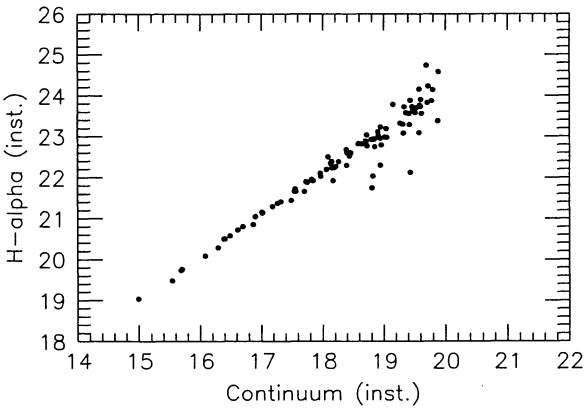

Fig. 14. Comparison of the magnitudes obtained with the Hα and nearby continuum filter. Stars located well below the trend probably have strong Hα emission.

the kinematic distance (6.1 ± 0.6 kpc) recently obtained by De Pree et al. (1999).

Figures 13a and 13b indicate that most of the massive stars have just evolved away from the ZAMS and that majority of the stars have age ≤ 1 Myr. Still, there are several stars whose age is as high as 5 Myr or more. This is in accordance with the fact that NGC 3603 contains three blue supergiants (Moffat 1983; Brandner et al. 1997) as well as three WN stars (Drissen et al. 1995). These stars must be older than 2 Myr. However, the age spread can be even larger, since we find some stars on the right side of the lower part of the ZAMS. The membership of these latter stars is examined on the basis of their distance from the cluster center and their reddening, as discussed in section 4, and a few of them are found to be probable members. These are marked as PMS in the last column of table 1a as well as in figures 13a and 13b. Recently, using infrared adaptive optics imaging, Eisenhauer et al. (1998) have shown the presence of a large number of pre–main-sequence stars of intermediate to low mass in NGC 3603. They derive an age of 0.3–1 Myr for these stars, which then are non-coeval with the majority of high-mass members. Thus, the NGC 3603 cluster apparently contradicts the widespread idea that star formation ceases after the formation of the most massive star in the cluster (cf. Herbig 1962; Herbst, Miller 1982; Larson 1982).

Brandner et al. (1997) have pointed out that the simultaneous presence of blue supergiants and stars of O3 type requires at least two distinct episodes of star formation in NGC 3603 separated by ≈ 10 Myr. The star formation in the NGC 3603 might have been initiated by the birth of the first generation of massive stars. Subsequently, they triggered the formation of the main star burst as well as a large number of lower-mass stars, through their interaction with dense cloud cores. Probably star formation in the NGC 3603 is still going on (Persi et al. 1985; Clayton 1990). A similar evolutionary scenario has been suggested by Hyland et al. (1992) to explain the starburst in the 30 Dor region.

Figure 14 compares the magnitudes obtained with the Hα and nearby continuum filters. The figure shows that most of the stars barring a few are distributed along a straight line. The stars lying below the line must have strong Hα emission. These stars are indicated in table 1a.

7. Discussions

The study of the reddening (figure 4) and stellar density (figure 5) within the NGC 3603 cluster indicates the presence of a region of low dust density at the center. In the case of 30 Dor, Brandl et al. (1996) have also

found that the stars in the core of the cluster show almost no extinction. A reasonable explanation for this is a lack of dust and gas in the central region, probably due to, e.g., a wind or supernova blown bubble. Clayton (1986) mentioned a 'stellar bubble' in NGC 3603 having a diameter of 50″ (2 pc) and a dynamical age of 10^4 yr; and it may have been created by the onset of the WR phase of three stars at the center (Drissen et al. 1995). The shells reported in the present work at radii $\sim 30''$ and $\sim 70''$ correspond to linear radii of ~ 0.9 pc and ~ 2.1 pc, respectively, at a distance of 6.3 kpc. The shell at radius $\sim 30''$ may correspond to the bubble mentioned by Clayton (1986). The mean extinction due to intra-cluster matter near to the center of the cluster (i.e., $r \sim 30''$) is $A_V \sim [4.3 \times \Delta E(B-V) =] 1.5$ mag. The extinction $A_V \approx 1$ mag corresponds to a gas column density of 6×10^{21} cm^{-2} (cf. Brandl et al. 1996), which on a scale of 1 pc corresponds to a gas density of 2000 cm^{-3}, a density not atypical inside young galactic giant H II regions (Brandl et al. 1996). Drissen et al. (1995) estimated that a minimum kinetic energy injected in the interstellar medium by stellar winds from the inner $r = 0.15$ pc of NGC 3603 is of the order of 10^{38} erg s^{-1} at the present time. Of this, roughly $\sim 1.7 \times 10^{34}$ erg s^{-1} have been sustained for about 2.5 Myr (cf., Drissen et al. 1995). A stellar wind of power $L_{\rm w}$ erg s^{-1} from a star located in a uniform cloud of neutral hydrogen density, n_0 atoms cm^{-3}, will in time 't' yr produce a spherical shell of diameter $D(t)$ pc, expanding at $V(t)$ km s^{-1}, where

$$L_{\rm w} = 9.5 \times 10^{17}\, n_0\, V(t)^5\, t^2 \quad \text{erg s}^{-1} \qquad (1)$$

$$D(t) = 3.5 \times 10^{-6}\, V(t)\, t \quad \text{pc} \quad \text{(cf. Clayton 1986).} \qquad (2)$$

By adopting a value of $V(t) \sim 70$ km s^{-1} (cf. Balick et al. 1980; Clayton 1986) and applying the above-mentioned equations for $L_{\rm w} \approx 3 \times 10^{38}$ erg s^{-1} (Drissen et al. 1995), we obtain the following parameters: $t \approx 10^4$ yr and $D(t) \approx 2.5$ pc. The diameter roughly corresponds to the first shell (at radius ~ 0.9 pc). The dynamical time scale of $\sim 10^4$ yr corresponds to the onset of the WR phase of the three central stars.

Goss and Radhakrishnan (1969) estimated the linear diameter to be ~ 17.9 pc and the H II mass to be $\sim 1.4 \times 10^4\, M_\odot$ for NGC 3603 using a distance of 8.4 kpc. These values are scaled to 13.4 pc and $\sim 0.8 \times 10^4\, M_\odot$ according to our distance of 6.3 kpc. The mass of the cluster within a diameter of 2 pc was estimated to be $M_* \sim 2.6 \times 10^3\, M_\odot$ by Eisenhauer et al. (1998), whereas, Brandner et al. (2000) have reported that the cluster mass is $\geq 4 \times 10^3\, M_\odot$. The star-formation efficiency (SFE) for the system, defined as the ratio of the total stellar mass and total stellar + gaseous masses, is thus estimated to be $\sim 25\%$. This should be considered to be the lower limit for the SFE, because we are using stellar mass within a diameter of only 2 pc. The star formation rate (SFR), obtained by dividing the mass of the cluster by the age of the cluster, comes out to be $\sim 2.6 \times 10^{-3}\, M_\odot$/yr. The total gas removal time can be estimated from

$$\tau \approx 1.5 \times (M_{\rm gas} \,/\, SFR),$$

where the factor of 1.5 compensates for the return of gas from massive stars back to the parental cloud as a result of stellar winds and supernovae (Sandage 1986). The gas-removal time turns out to be 4.6 Myr.

The gas-removal time is an important parameter, because it determines the fate of the cluster, i.e., whether the cluster would be a bound or unbound system. Bound cluster systems result in the case that the molecular clouds from which these systems are formed are either dispersed slowly after a appearance of the cluster, or that the cloud attains a SFE of about 50% or higher if the cloud disruption is sudden (cf. Pandey et al. 1990 and references therein). Lada et al. (1984) have theoretically obtained that molecular clouds with $SFE > 21\%$ can produce bound open cluster systems if the gas-removal time, τ, is considered to be about 5 Myr or longer, which appears to apply to NGC 3603.

8. Conclusions

From the two-colour diagram and variable extinction analysis, the extinction law for the dust inside the cluster NGC 3603 is found to be abnormal, having $R = 4.3 \pm 0.2$. By combining this with the normal value of R for the normal foreground reddening, the distance modulus turns out to be ~ 14.0, which corresponds to a distance of 6.3 kpc. This distance is smaller than those obtained in previous studies (cf. Melnick et al. 1989).

From the colour–magnitude diagram (figures 10a and 10b) we find that the mean age of the cluster is ≤ 1 Myr, and that the cluster has some age spread, having a few stars as old as up to several Myr. The present work supports the concept of continuous star formation in the cluster NGC 3603. The fact that a few stars having masses of $5 < M/M_\odot < 15$ are still in the PMS phase casts doubt on the standard notion that after the formation of most massive star(s) the star-formation processes ceases. We estimate a minimum star formation efficiency of $\sim 25\%$ in the cluster.

The authors are thankful to Drs R. Sagar and H. C. Bhatt for useful discussions and suggestions. A. K. Pandey is thankful to the Department of Science and Technology (India) for providing financial assistance under the grant No. SP/S2/O-07/93.

References

Balick B., Boeshaar G.O., Gull T.R. 1980, ApJ 242, 584

Brandl B., Sams B.J., Bertoldi F., Eckrat A., Genzei R., Drapatz S., Hofmann R., Löwe M. 1996, ApJ 466, 254
Brandner W., Grebel E.K., Chu Y.-H., Dottori H., Brandl B., Richling S., Yorkee H.W., Points S.D. 2000, AJ 119, 292
Brandner W., Grebel E.K., Chu Y.-H., Weis K. 1997, ApJ 475, L45
Chini R., Krügel E. 1983, A&A 117, 289
Chini R., Wargau W.F. 1990, A&A 227, 213
Clayton C.A. 1986, MNRAS 219, 895
Clayton C.A. 1990, MNRAS 246, 712
De Pree C.G., Nysewander M.C., Goss W.M. 1999, AJ 117, 2902
Drissen L., Moffat A.F.J., Walborn N.R., Shara M.M. 1995, AJ 110, 2235
Eisenhauer F., Quirrenbach A., Zinnecker H., Genzel R. 1998, ApJ 498, 278
Goss W.M., Radhakrishnan V. 1969, Astrophys. Lett. 4, 199
Herbig G.H. 1962, ApJ 135, 736
Herbst W., Miller D.P. 1982, AJ 87, 1478
Hofmann K.-H., Seggewiss W., Weigelt G. 1995, A&A 300, 403
Hyland A.R., Straw S., Jones T.J., Gatley I. 1992, MNRAS 257, 391
Johnson H.L., Morgan W.W. 1953, ApJ 117, 313
Lada C.J., Margulis M., Dearborn D. 1984, ApJ 285, 141
Larson R.B. 1982, MNRAS 200, 159
Maeder A., Meynet G. 1987, A&A 182, 243
Melnick J., Grosbøl P. 1982, A&A 107, 23
Melnick J., Tapia M., Terlevich R. 1989, A&A 213, 89
Mermilliod J.C. 1981, A&A 97, 235
Moffat A.F.J. 1983, A&A 124, 273
Moffat A.F.J., Drissen L., Shara M.M. 1994, ApJ 436, 183
Moffat A.F.J., Seggewiss W., Shara M.M. 1985, ApJ 295, 109
Neckel Th., Chini R. 1981, A&AS 45, 451
Ogura K., Ishida K. 1981, PASJ 33, 149
Pandey A.K., Mahra H.S., Sagar R. 1990, AJ 99, 617
Persi P., Tapia M., Roth M., Ferrari-Toniolo M. 1985, A&A 144, 275
Sagar R., Piskunov A.E., Myakutin V.I., Joshi U.C. 1986, MNRAS 220, 383
Sandage A. 1986, A&A 161, 89
Schmidt-Kaler Th. 1982, in Landolt-Börnstein, Neue Serie Gr.VI, Vol 2b (Springer, Berlin, Heidelberg, New York) p19
Selman F., Melnick J., Bosch G., Terlevich R. 1999, A&A 341, 98
Sher D. 1965, MNRAS 129, 237
Turner D.G. 1976, AJ 81, 97
van den Bergh S. 1978, A&A 63, 275